

# Broad Spiral-Bandwidth of Orbital Angular Momentum Interface between Photon and Memory

Dong-Sheng Ding,<sup>1,2,\*</sup> Ming-Xin Dong,<sup>1,2</sup> Wei Zhang,<sup>1,2</sup> Shuai Shi,<sup>1,2</sup>  
Yi-Chen Yu,<sup>1,2</sup> Ying-Hao Ye,<sup>1,2</sup> Guang-Can Guo,<sup>1,2</sup> and Bao-Sen Shi<sup>1,2,†</sup>

<sup>1</sup>Key Laboratory of Quantum Information, University of Science and Technology of China, Hefei, Anhui 230026, China.

<sup>2</sup>Synergetic Innovation Center of Quantum Information and Quantum Physics,  
University of Science and Technology of China, Hefei, Anhui 230026, China.

(Dated: February 15, 2019)

The complex interactions between orbital angular momentum (OAM) light and atoms are particularly intriguing in the areas of quantum optics and quantum information science. Building a versatile high-dimensional quantum network needs broad spiral-bandwidth for preparing higher-quanta OAM mode and resolving the bandwidth mismatch in spatial space and etc. Here, we experimentally demonstrate a broad spiral-bandwidth quantum interface between photon and memory. Through twisted fields of the writing and reading, the correlated OAM distribution between photon and memory is significantly broadened. This broad spiral-bandwidth quantum interface could be spanned in multiplexing regime and could work in high-quanta scenario with capability of  $|l| = 30$ , and we demonstrate the entanglement within 2-D subspace with a fidelity of  $80.5 \pm 4.8\%$  for high  $l$ . Such state-of-the-art technology to freely control the spatial distribution of OAM memory is very helpful to construct high-dimensional quantum networks and provides a benchmark in the field of actively developing methods to engineer OAM single photon from matters.

The interaction between orbital angular momentum (OAM) of structured light and matters has many intriguing applications [1], including trapping of particles [2, 3] and measuring rotation angular [4, 5], OAM-based imaging [6] and optical communications [7]. In quantum information field, light carried with OAM could significantly enhance the information capacity, thus advancing the developments of the high-dimensional (high-D) quantum networks, especially in OAM entanglement generation [8–11], OAM-based quantum memory [12–18] and OAM-based teleportation [19]. One of strumbling block of constructing a high-D quantum network is how to establish a versatile high-D OAM quantum interface between photon and memory [20].

Building a high-D OAM quantum interface could be based on the protocol of Duan-Lukin-Cirac-Zoller (DLCZ) [21] where the probabilistically generated OAM photon is entangled with memory [12, 22]. There are many parameters to characterize the performance of the interface between photon and memory [23, 24], such as lifetime, efficiency and fidelity and etc [24–26]. The most unique parameter of high-D OAM quantum interface could be spiral-bandwidth  $\delta l$ , which characterizes the mode-matching bandwidth window [27]. The adjacent nodes in high-dimensional quantum networks may be diverse and different in spatial mode, spiral-bandwidth and etc, for example, one is encoded in  $\pm l$  OAM spaces and the other one is in  $\pm(l + m)$  OAM spaces; or one has the spatial-bandwidth of  $\delta l$  and another is  $\delta(l + m)$ , thus needing a technology to make the quantum interface be more flexible and controllable and then people can connect them freely [28].

In this letter, we experimentally demonstrate a high-D OAM interface between photon and memory in delayed

spontaneously four-wave mixing process. In this configuration, the write- and read-laser beams are individually encoded, thus making the joint of correlation against  $l$  modes broadened because the interaction length is increased in transverse azimuthal direction. This offers the ability to control the spatial distribution, including entangled OAM eigenmode  $\pm l$  and the spiral-bandwidth  $\delta l$ . Based on that, we demonstrate the potential applications for OAM multiplexing, and give an obvious contrast data with inputting  $\Delta l = 10$ . We also have achieved high-D entanglement with  $l$  up to 16 and high-quanta 2-dimensional OAM entanglement with  $l$  up to 30, all of which obey the entanglement properties. The reported results are useful for realizing broad spiral-bandwidth and high-D quantum memory and increasing the capacity of quantum communication, and also is a benchmark of searching ways to explore versatile quantum interfaces.

The experimental media is an optically thick atomic ensemble of Rubidium 85 ( $^{85}\text{Rb}$ ) that is trapped in two-dimensional magneto-optic trap (MOT). The involved schematic of the energy levels and the experimental setup are shown in Fig. 1(a) and Fig. 1(b). We firstly establish the correlation between a collective spin excited state (spin wave, also called as atomic memory) and a single photon (Signal 1) through spontaneous Raman scattering (SRS) in atomic ensemble. In this process, the write-laser is set to blue-detuned with atomic transition  $|2\rangle \rightarrow |3\rangle$ . After reflecting from SLM 1 as depicted in Fig. 1 (b), the write-laser has carried on the OAM phase message loaded by a computer. Then, a 4-f image system with unequal arms, which is consisted of two lenses L1 and L2 with focal length of 300 mm and 500 mm respectively, is utilized to map the OAM phase of the write-laser to the center of atomic ensemble accurately. The Signal 1 photon emit-

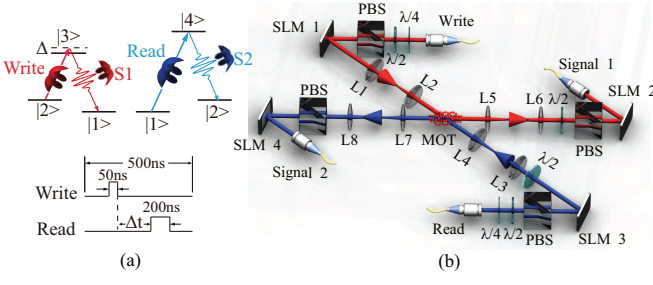


Figure 1. Overview of experiment. (a) The relevant energy level diagram. Write and Read represent write-laser pulse and read-laser pulse respectively; S1 and S2 are Signal 1 photon and Signal 2 photon. States  $|1\rangle$ ,  $|2\rangle$ ,  $|3\rangle$  and  $|4\rangle$  correspond to  $^{85}\text{Rb}$  atomic levels of  $5S_{1/2}(F=2)$ ,  $5S_{1/2}(F=3)$ ,  $5P_{1/2}(F=3)$  and  $5P_{3/2}(F=3)$  respectively.  $\Delta$  represents the detuning of write-laser pulse, which is set to be  $+70 \times 2\pi$  MHz. The part in below is the time sequence of experiment. (b) Experimental setup. MOT is magneto-optical trap,  $L1 - L8$  represent a series of lenses,  $\lambda/4$  is quarter-wave plate,  $\lambda/2$  is half-wave plate and PBS is polarization beam splitter. SLM 1 ~ 4 are spatial light modulators.

ted from atomic ensemble is mapped onto another SLM 2 for detecting the OAM modes. Due to the angular momentum is conserved in SRS process, hence the spatial modes of the spin wave and Signal 1 are entangled in OAM degree of freedom. This OAM correlation can be flexibly demonstrated by mapping and checking the OAM modes on SLM 1 and SLM 2 respectively.

The OAM-based DLCZ quantum memory is built when the entanglement between the spin wave and Signal 1 photon is created. After a storage time of  $\Delta t$ , we use another SLM 3 to load OAM structured light to read the spin wave out to Signal 2, the Signal 2 is also mapped onto another SLM 4. Ultimately, in order to check the quantum correlation between Signal 1 and atomic spin wave, we measure the coincidence counts between Signal 1 and Signal 2 by projecting them onto SLM 2 and SLM 4 respectively, in which the different phase structures on both of SLM 2 and 4 are loaded for measurement. Here, two couples of 4-f systems with unequal arms are used to map the OAM phase of signal photons to SLM accurately, see supplementary information. The reflected photons from SLMs are collected into two single-mode fibers, which are detected by two detectors (avalanche diode, PerkinElmer SPCM-AQR-16-FC, 60% efficiency, maximum dark count rate of 25/s) respectively.

In previous work [17] for demonstrating high-D OAM quantum interface with Gaussian mode input, it is hard to generate higher-D entanglement because the correlated coincidences of photons decay very quickly against  $l$ . Here, we turn the OAM quanta of write- and read-beams to modulate the light-atom interaction length. We input the write-laser with OAM quanta of  $l_W$ . Due to the fact that SRS process conserves angular momentum, we have created OAM entanglement between Signal 1 and

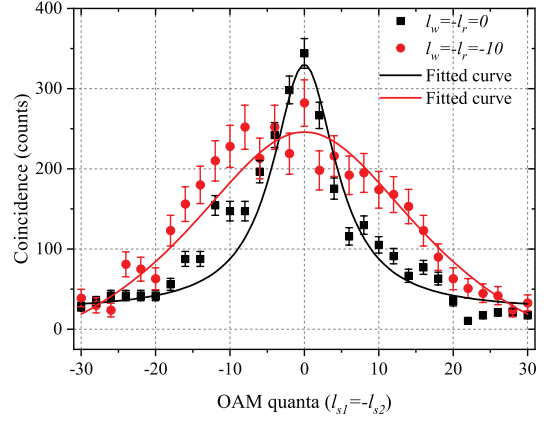


Figure 2. The measured correlated OAM distribution under different OAM modes of write- and read-beams. The correlated OAM distribution with  $l_w = -l_r = 0$  (black line) and  $l_w = -l_r = 10$  (red line). These data are fitted by the function  $y = y_0 + 2aw / [\pi(4x^2 + w^2)]$  with parameters ( $y_0 = 15.8$ ,  $w = 11.4 \pm 2.3$ ,  $a = 5501$ ) and ( $y_0 = 0$ ,  $w = 27.0 \pm 1.8$ ,  $a = 11534$ ).

atomic memory, which can be specified by the formula

$$|\psi\rangle_{\text{photon-atom}}^{l_w} = \sum_{l=-\infty}^{l=\infty} c_l |l\rangle_{S1} \otimes |l_W - l\rangle_a \quad (1)$$

here,  $|c_l|^2$  represents excitation probability,  $|l\rangle_{S1}$  is the OAM eigenmode of Signal 1 with quanta of  $l$ .  $|l_W - l\rangle_a$  is the OAM eigenmode of atomic memory with quanta of  $l_W - l$ . Through this method, the atomic memory could carry the arbitrary OAM topological charge with the term of  $l_W - l$ , thus resulting in the redistributed quantum interface. We also check the conservation of OAM modes at two situations  $l_W = 2$ ,  $l_R = 0$  and  $l_W = 1$  and  $l_R = 2$ , which can be found in the supplement. Most importantly, the spiral-bandwidth of generated photons is broadened when we increase the OAM quanta of write- and read-beams.

Due to the broadening effect of spiral-bandwidth with larger  $l$  laser beam input, the distribution of generated OAM signal 1 and memory would be redistributed in more flat range. This is because the generated OAM modes are dependent on the interaction length and the waist of the write- and read-beams [29]. The vector mismatching  $\Delta k$  from transverse azimuthal phase would increase the value of  $\Delta k \cdot L$ , where  $L$  is the interaction length. This effect is very promising because it is regarded as a concentration operation. In order to achieve high-D OAM quantum memory, we utilize the above method to extend the quanta of write-laser, we set  $l_W = 10$ . In addition, we set  $l_R = -10$  for reading process. The writing and reading process of DLCZ quantum memory is essentially a delayed spontaneously four-wave mixing process. Based on the unique advantages of individually modulating write- and read-beams

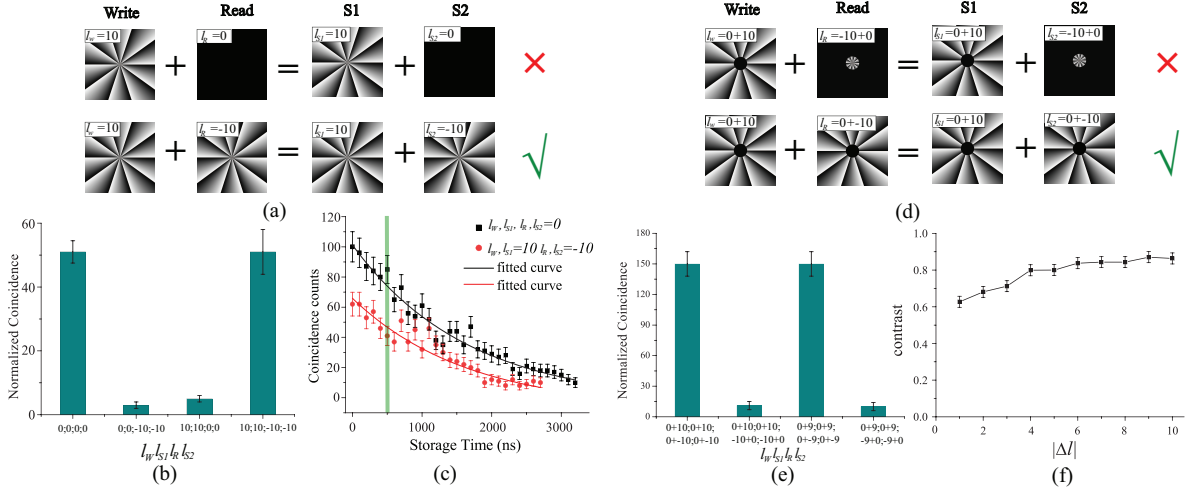


Figure 3. Multiplexing OAM modes. (a) The multiplexing with different OAM modes of write- and read-lasers. The cross and check marks in up/down equation shows the weak/strong correlation under the different ( $|l_W| \neq |l_R|$ ) /same OAM orders ( $|l_W| = |l_R|$ ). (b) The coincidence counts for the different situations of  $|l_W| = |0\rangle/|10\rangle$ ,  $|l_{S1}| = |0\rangle/|10\rangle$ ,  $|l_R| = |0\rangle/|-10\rangle$ ,  $|l_{S2}| = |0\rangle/|-10\rangle$ . (c) The memory decay function with different OAM modes (black for  $|l_W| = 0$ , red for  $|l_W| = 10$ ). The memory decays exponentially with coherence time of  $\tau = 1655$  ns. (d) The multiplexing in radial direction with different OAM modes in inner and outer rings. When the OAM orders in the inner and outer rings are different (up equation), the correlation is weak; On the contrary, the correlation is strong when the OAM orders are same (down equation). (e) The normalized coincidence counts with  $|l_W\rangle = |0\rangle + |10\rangle$ ,  $|l_R\rangle = |-10\rangle + |0\rangle$  and  $|l_W\rangle = |0\rangle + |10\rangle$ ,  $|l_R\rangle = |0\rangle + |-10\rangle$  in the left two bars. The right two bars are the corresponding OAM mode of  $|l_W\rangle = |0\rangle + |9\rangle$ ,  $|l_R\rangle = |-9\rangle + |0\rangle$  and  $|l_W\rangle = |0\rangle + |9\rangle$ ,  $|l_R\rangle = |0\rangle + |-9\rangle$ . (f) The detected contrast of coincidence counts against different  $\Delta l$ . The storage time is set to be 500 ns. The different signs of OAM quanta set in (a) and (d) are required to maintain OAM conservation.

of four-wave mixing process (not like a single pump field used in spontaneous parametric down conversion), the write- and read-laser beams can be individually loaded OAM modes with opposite signs whilst the input total angular momentum can be zero, thus making the joint spectrum of correlation broadened. We map different OAM phases onto SLM 2 and SLM 4, and record the coincidence between Signal 1 and Signal 2 photons. The spiral-bandwidth of OAM entanglement is measured in the red line in Fig. 2. The spiral-bandwidth of generated single photons becomes much flat than the scheme with inputting Gaussian mode. The spiral-bandwidth of Gaussian mode is about  $\delta l = 11.4 \pm 2.3$ , whilst for  $l_W = -l_R = 10$  the spiral-bandwidth is  $\delta l = 27.0 \pm 1.8$  obviously enhanced by a factor of  $\sim 2.4$ . We also check the high-D OAM entanglement with the broadened spiral-bandwidth, and give a high-D entanglement properties with OAM quanta up to  $\Delta l = 16$ , see supplement.

With increasing the OAM quanta in DLCZ writing and reading processes, we exhibit a potential application for multiplexing with different OAM modes. If we select  $l_W = 10$  for writing and  $l_R = -10$  for reading out, we can detect the correlated coincidence; while for  $l_W = 10$ ,  $l_R = 0$  given in Fig. 3(a), there would be almost no coincidence counts exhibiting orthogonality-like property shown by Fig. 3(b). The nonlinearity of the interleaved OAM modes is strongly dependent on the overlap of beam profiles of write- and read-beams,

it would become small if the mismatch between write- and read-beams is large, then the coincidence counts would jump down, see supplement. The detected contrast  $(C_{\text{same}} - C_{\text{diff}})/(C_{\text{same}} + C_{\text{diff}})$  is  $0.85 \pm 0.03$  (where  $C_{\text{same}}$  and  $C_{\text{diff}}$  are defined as coincidence counts with same ( $|l_W| = |l_R|$ ) and different ( $|l_W| \neq |l_R|$ ) write- and read-beam OAM modes), near to the theoretical estimation of 0.91. In this process, the storage coherence time is almost same for  $l_W = 0$  and  $l_W = 10$ , see Fig. 3(c). Furthermore, we map the different OAM modes in the inner ( $l_{in}$ ) and outer rings ( $l_{out}$ ) to detect the multiplexing property along radial direction, see Fig. 3(d). Since the nonlinearity of interleaved OAM modes (for example  $l_W = 0$  and  $l_W = 10$ ) in the center of ensemble can be distinguished by inputting distinct OAM modes (Fig. 3(e)), this may result in multiplexing along radial direction. We map the different OAM modes with  $\Delta l = 1, 2, \dots, 10$  in inner and outer rings ( $\Delta l = l_{out} - l_{in}$ ) and detect the correlation given in Fig. 3(e). The crosstalk between different OAM modes is detected by setting same phase structure or the different phase structure. The contrast of coincidence counts is increased against with  $\Delta l$  because the large difference  $\Delta l$  means that the mismatch between write- and read-beams decrease the correlation (Fig. 3(f)), agreeing with the above analysis. This whole process could be regarded as the multiplexing of two OAM spectra, which are created by inputting two distinct OAM writing and reading ( $l_{out}$ ,  $l_{in}$ ), thus

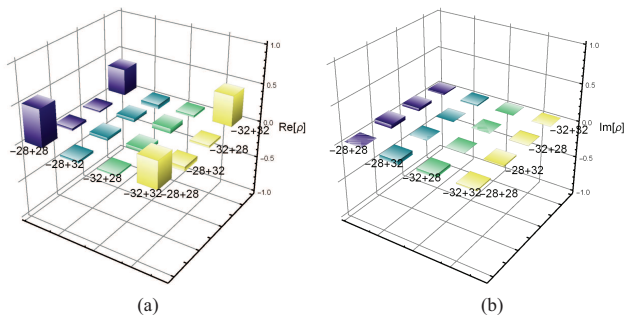


Figure 4. The reconstructed density matrix for photonic entangled state  $|\psi\rangle_{\text{photon-photon}}^{30,-30}$ . (a) and (b) are the real and imaginary parts of density matrix respectively. Each data for reconstructing density matrices are recorded in 3000 s

satisfying some quantum information protocols with one OAM spectra docking to another OAM spectra.

At last, broad spiral-bandwidth offers an ability for demonstrating high-quanta OAM quantum interface in 2-D subspace. For this, we set  $l_W = 30$ ,  $l_R = -30$ , the storage time is set to be twice of the width of write pulse, the decoherence from the transverse azimuthal momentum mismatch between write-laser and the Signal 1 photons is ignored. The nonlinearity of the DLCZ process at large quanta  $l$  is relatively small, we then only consider the two OAM modes for verifying entanglement. We choose the OAM modes of  $l = 28, 32$  to verify the high-quanta OAM entanglement. The photonic entangled state is expressed as:

$$|\psi\rangle_{\text{photon-photon}}^{30,-30} = \frac{1}{\sqrt{2}} (| -28 \rangle_{S1} | 28 \rangle_{S2} + | -32 \rangle_{S1} | 32 \rangle_{S2}) \quad (2)$$

Through quantum state tomography, we obtain the reconstructed density matrix as shown in Fig. 4(a) and (b). The fidelity of reconstructed density matrix is calculated as  $80.5 \pm 4.8\%$  by comparing with the ideal density matrix. We also check the violation of Clauser-Horne-Shimony-Holt (CHSH) inequality [30–32] to demonstrate the nonlocality of the entangled state. The CHSH parameter  $S$  [33] is represented as following:  $S = |E(\theta_{S2}, \theta_{S1}) - E(\theta_{S2}, \theta'_{S1}) + E(\theta'_{S2}, \theta_{S1}) + E(\theta'_{S2}, \theta'_{S1})|$ . Here, the correlation function  $E(\theta_{S2}, \theta_{S1})$  can be calculated from the rates of coincidence at several particular orientations,  $\theta/\theta'$  represents the angle of phase distribution on the surface of SLM 2 and SLM 4. The calculated  $S$  is  $2.22 \pm 0.07$  which is larger than 2 violating the CHSH inequality, thus it demonstrates the real entanglement between Signal 1 and Signal 2 photons.

In this work, we demonstrate a broad spiral-bandwidth OAM DLCZ memory, the OAM distribution and the quanta of OAM quantum interface are freely manipulated. In this state-of-the-art quantum interface, we have achieved high-D OAM entanglement with OAM modes

difference  $\Delta l$  up to 16, the quanta of OAM 2-D subspace can be accessible to  $l = \pm 30$ . The experiment reported here would be very promising to demonstrate high-quanta OAM quantum interface and study the fundamental physics in OAM-based light and matter interaction.

## ACKNOWLEDGMENTS

Dong-Sheng Ding and Ming-Xin Dong contributed this paper equally. We thank Guo-Yong Xiang professor for loaning a SLM. This work was supported by National Key R&D Program of China (2017YFA0304800), the National Natural Science Foundation of China (Grant Nos. 61525504, 61722510, 61435011, 11174271, 61275115, 11604322), and the Innovation Fund from Chinese Academy of Sciences.

## SUPPLEMENTARY

### Experimental time sequence.

The repetition rate of our experiment is 100 Hz, and the MOT trapping time is 8.7 ms. Besides, the operation window of 1.3 ms consists of 2600 cycles with a cycle time of 500 ns. Write-laser and read-laser are pulsed by acousto-optic modulator with pulse width of 50 ns and 200 ns respectively in each cycle. The optical depth in MOT is about 40. The storage time is controlled by changing the delay time between write- and read-laser through an arbitrary function generator. The magnetic field for trapping is shut down in the experiment window.

### 4-F image system for four SLMs.

The SLM 1 acts as a mask plane, and the center of atomic ensemble in MOT is the image plane. Two lenses L1 and L2 with focal length of 300 mm and 500 mm are utilized to map the phase message of SLM 1 to the atomic ensemble. Due to the phase matching condition  $k_W - k_{S1} = k_R - k_{S2}$ , the imaging system can be easily optically aligned. The Signal 1 and Signal 2 fields are collinear, the Signal 1 beam is completely overlapped by the write beam through demonstrating electromagnetically induced transparency effect. Here, the write-laser carrying high OAM quanta diffracts very strongly and results in the waist of laser beam too large in the center of atomic ensemble, which results in weak interaction between write-laser and atomic ensemble. Through the 4-f image system with unequal arms, we can not only map the OAM phase message to the center of atomic ensemble accurately but also decrease the waist of write-laser



with high OAM quanta. Similarly, the single photon carried with OAM phase message from the center of atomic ensemble is retrieved to project on SLM 1 via the other 4-f image system, and ultimately we collect photons by single-mode fibers.

### Theoretical analysis.

In the interaction picture, despite the decay of spin wave, the effective Hamiltonian for the delayed four-wave mixing process is written as [34]

$$\hat{H}_I = \frac{\varepsilon_0}{4} \int_{-L/2}^{L/2} dz \chi^{(3)} \vec{E}_W \vec{E}_R \vec{E}_{S1}^* \vec{E}_{S2}^* + H.c \quad (3)$$

where  $H.c.$  means the Hermitian conjugate.  $\chi^{(3)}$  is the third-order nonlinear susceptibility for resonant signal 2 photon, which is given [35]:

$$\chi^{(3)} = \frac{N\mu_{13}\mu_{32}\mu_{24}\mu_{41}/(\varepsilon_0\hbar^3)}{(\Delta_W + i\gamma_{23})[\Omega_R^2 - 4(\omega + i\gamma_{24})(\omega + i\gamma_{21})]} \quad (4)$$

here,  $\mu_{ij}$  are the electric dipole matrix elements.  $\gamma_{ij}$  are the dephasing rates.  $\Omega_R$  is the Rabi frequency of read laser. The probability to generate the Signal 1 and Signal 2 in modes  $|l_{S1}\rangle$ ,  $|l_{S2}\rangle$  is given by the overlap with write- and read-laser beam profiles:

$$c_{l_W l_R l_{S1} l_{S2}} \sim \int_{-L/2}^{L/2} \int_0^r \int_0^{2\pi} \varepsilon_0 \chi^{(3)} r LG_0^{l_W}(r, \phi) LG_0^{l_R}(r, \phi) LG_0^{l_{S1}}(r, \phi) [LG_0^{l_{S2}}(r, \phi)]^* d\phi dr dz \quad (5)$$

The integral over the azimuthal coordinate is

$$\int_0^{2\pi} d\phi \exp[i(l_W + l_R - l_{S1} - l_{S2})\phi] = 2\pi \delta_{l_W + l_R, l_{S1} + l_{S2}} \quad (6)$$

From which, we can obtain the topological charge conservation law in OAM space is  $l_W + l_R = l_{S1} + l_{S2}$ . According to Eq. (4), we can find the probability of  $l_{S1}$ -Signal 1 and  $l_{S2}$ -Signal 2 photons with  $l_W$ -write and  $l_R$ -read lasers, which strongly depends on the profiles match between the four fields.

In order to illustrate the topological charge conservation law in our OAM quantum interface in DLCZ memory, we input the write-laser with OAM quanta of  $l_W$ . Due to the fact that SRS process conserves angular momentum, we have created OAM entanglement between Signal 1 and atomic spin wave, which can be specified

by the formula  $|\psi\rangle_{\text{photon-atom}}^{l_W} = \sum_{l=-\infty}^{l=\infty} c_l |l\rangle_{S1} \otimes |l_W - l\rangle_a$ , here,  $|c_l|^2$  represents excitation probability,  $|l\rangle_{S1}$  is the OAM eigenmode of Signal 1 with quanta of  $l$ .  $|l_W - l\rangle_a$  is the OAM eigenmode of atomic spin wave with quanta of  $l_W - l$ . Through this method, the atomic spin wave could carry the arbitrary OAM topological charge with the term of  $l_W - l$ , thus resulting in the redistributed quantum interface.

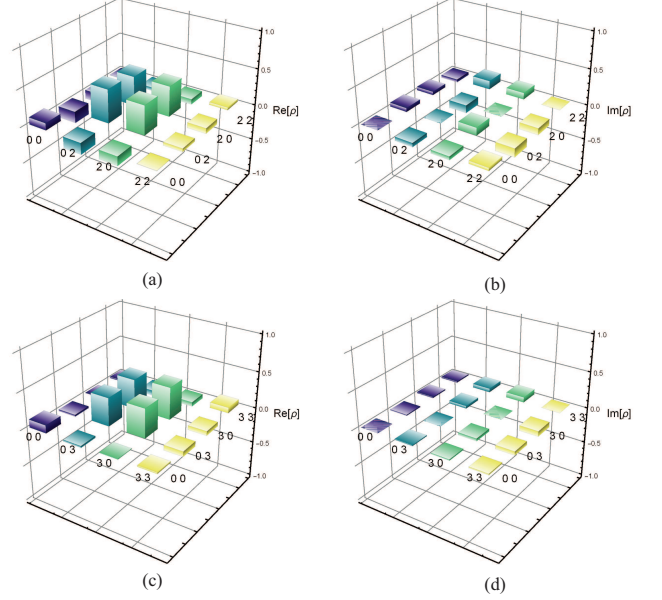


Figure 5. Reconstructed density matrices for Modulated OAM entanglement. The real (a,c) and imaginary (b, d) parts of density matrices for photonic OAM entangled state  $|\psi\rangle_{\text{photon-photon}}^{2,0}$  and  $|\psi\rangle_{\text{photon-photon}}^{1,2}$ . Each data for reconstructing density matrices are recorded in 1000 s.

After a period of storage, we check photon-atom entanglement by inputting read-laser with OAM quanta of  $l_R$ , and checking the entanglement between Signal 1 and Signal 2. The entanglement between Signal 1 and Signal 2 can be written as  $|\psi\rangle_{\text{photon-photon}}^{l_W, l_R} = \sum_{l=-\infty}^{l=\infty} c_l |l\rangle_{S1} \otimes |l_W + l_R - l\rangle_{S2}$ . At first, we set  $l_W = 2$  and  $l_R = 0$ , it means using OAM quanta of 2 and 0 to write and read respectively. Thus, the photonic entangled state is a sum of  $|l\rangle_{S1} \otimes |2 - l\rangle_{S2}$  with different  $l$ , this is a modulated asymmetric OAM entangled state. Here, we only post-select the OAM mode of entangled state into two-dimensional subspace  $|0\rangle_{S1}|2\rangle_{S2}$  and  $|2\rangle_{S1}|0\rangle_{S2}$ , that is  $|\psi\rangle_{\text{photon-photon}}^{2,0} = 1/\sqrt{2} (|0\rangle_{S1}|2\rangle_{S2} + |2\rangle_{S1}|0\rangle_{S2})$ . To characterize the OAM entanglement between Signal 1 and Signal 2, we reconstruct the density matrices by projecting Signal 1 and Signal 2 onto OAM bases of  $|0\rangle$ ,  $|2\rangle$ ,  $(|0\rangle - i|2\rangle)/2^{1/2}$ ,  $(|0\rangle + |2\rangle)/2^{1/2}$  for demonstrating quantum tomography. Then we use the obtained 16 coincidence rates to reconstruct the density matrix of state as shown in Fig. 5 (a) and (b). According to the formula  $F = \text{Tr}(\sqrt{\sqrt{\rho}\rho_{\text{ideal}}\sqrt{\rho}})^2$ , which

compares the constructed density matrix  $\rho$  with the ideal density matrix  $\rho_{\text{ideal}}$ , we obtain the fidelity of  $83.3 \pm 3.5\%$ . We also try another data set of  $m_1 = 1$  and  $m_2 = 2$ , and obtain the photonic entangled state  $|\psi\rangle_{\text{photon-photon}}^{1,2} = 1/\sqrt{2}(|0\rangle_{S1}|3\rangle_{S2} + |3\rangle_{S1}|0\rangle_{S2})$ . Similarly, we reconstruct the density matrix of this state, the real and imaginary parts of reconstructed density matrix are shown in Fig. 5 (c) and (d), with fidelity of  $81.1 \pm 4.2\%$ . In this process, although the fidelity is not very high, but it reveals that in DLCZ quantum memory, the OAM modes are conserved in the whole writing and reading process.

### The entanglement dimensionality witness.

In order to demonstrate the high-D entanglement between Signal 1 and atomic memory, we avoid the crosstalk between neighboring OAM modes. We select the modes of  $l = 0, 4, 8, 12, 16$  in which three modes between adjacent terms are removed for better isolation. We read the photon-atom entanglement out to photon-photon entanglement for verification. So, the entangled state is  $|\psi\rangle_{\text{photon-photon}}^{10,-10} = c_1|0\rangle_{S1}|0\rangle_{S2} + c_2|-4\rangle_{S1}|4\rangle_{S2} + c_3|-8\rangle_{S1}|8\rangle_{S2} + c_4|-12\rangle_{S1}|12\rangle_{S2} + c_5|-16\rangle_{S1}|16\rangle_{S2}$  here,  $c_5 \sim c_5$  are the corresponding amplitudes of different terms  $|0\rangle_{S1}|0\rangle_{S2} \sim |-16\rangle_{S1}|16\rangle_{S2}$ . For verifying the high-D state, it is very promising to use high-D entanglement dimensionality witness Krenn *et al.* [11], Agnew *et al.* [36] to characterize the entanglement existed in our system. The entanglement dimensionality witness is expressed as  $W_d = 3\frac{D(D-1)}{2} - D(D-d)$ , here,  $D$  is the number of measured OAM modes, and  $d$  is associated with dimensions of entanglement. If  $W > W_d$ , the two photons entangled in at least  $d+1$  dimensions, where  $W$  is obtained from calculating the sum of visibilities  $N = V_x + V_y + V_z$  in total two dimensional subspace. The  $V_x, V_y$  and  $V_z$  represent the visibilities of two-photon interference in the diagonal/anti-diagonal, left-circular/right-circular and horizontal/vertical bases respectively in each OAM mode of  $a$  and  $b$ , here  $a$  and  $b$  are selected from  $l = 0, 4, 8, 12, 16$ . A disadvantage of quantum tomography for high-D entanglement is that the needed measurement data is the order of  $d^4$ , which is a large challenge in its realization and is impractical while  $d$  is set to 5 in our experiment. Therefore, we adopt the method of dimensionality witness to certificate the existence of high-D entanglement and characterize the dimensionality. We calculate the value  $W$  is  $21.93 \pm 0.55$ , which violates the bound  $W_d$  of 20 (the number of measured OAM mode  $D$  is 5 and  $d$  is 3) by 3 s.d's, thus there is at least a 4-D OAM entanglement between Signal 1 and Signal 2 photons. In these measurements, the atom-photon entangled states are both detected in photonic regime, we assume the fidelity of reading out from ensembles is near unit. Although there are definitely some

noise or inefficient elements from reading process, making the degree of the measured entanglement lower than that existed in ensembles.

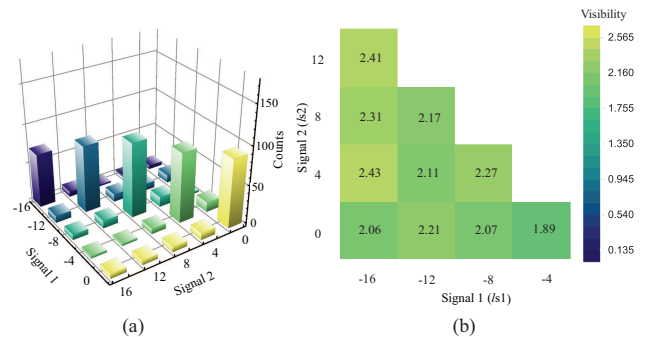


Figure 6. (a) The post-selected correlated OAM matrix between Signal 1 and Signal 2 photons with OAM modes difference  $|\Delta l|$  up to 16. (b) The each sum of visibilities for 2-D subspaces for detecting the high-D entanglement dimensionality witness.

### 2-D high- $l$ Entanglement and state tomography

If we considered the OAM modes of  $a$  and  $b$  with  $l=32$  and 28, the Signal 1 and Signal 2 are entangled in OAM space and entangled state is expressed as

$$|\Psi_3\rangle = 1/\sqrt{2}(|-28\rangle_{S1}|28\rangle_{S2} + |-32\rangle_{S1}|32\rangle_{S2}) \quad (7)$$

Here,  $|-28\rangle_{S1}$  represents the Signal 1 carrying with OAM quanta of -28. By using two computers, we project two photons onto two SLMs respectively and four state of  $|\phi_{1\sim 4}\rangle$  ( $|-28\rangle, |-32\rangle, (|-28\rangle - i|-32\rangle)/2^{1/2}, (|-28\rangle + |-32\rangle)/2^{1/2}$ ) are programmed onto SLM 2 and  $|\varphi_{1\sim 4}\rangle$  ( $|28\rangle, |32\rangle, (|28\rangle - i|32\rangle)/2^{1/2}, (|28\rangle + |32\rangle)/2^{1/2}$ ) are programmed onto SLM 4. Then, we obtain a set of 16 data for reconstructing the density matrix given in the main text. The error bars in our experiment are estimated by Poisson statistics and using Monte Carlo simulations with the aid of Mathematica software.

\* [dds@ustc.edu.cn](mailto:dds@ustc.edu.cn)

† [drshi@ustc.edu.cn](mailto:drshi@ustc.edu.cn)

- [1] Miles J Padgett, "Orbital angular momentum 25 years on," *Optics Express* **25**, 11265–11274 (2017).
- [2] H He, MEJ Friese, NR Heckenberg, and H Rubinsztein-Dunlop, "Direct observation of transfer of angular momentum to absorptive particles from a laser beam with a phase singularity," *Physical Review Letters* **75**, 826 (1995).
- [3] Xiaodong He, Peng Xu, Jin Wang, and Mingsheng Zhan, "Rotating single atoms in a ring lattice generated by a spatial light modulator," *Optics Express* **17**, 21007–21014 (2009).

- [4] J Courtial, K Dholakia, DA Robertson, L Allen, and MJ Padgett, “Measurement of the rotational frequency shift imparted to a rotating light beam possessing orbital angular momentum,” *Physical review letters* **80**, 3217 (1998).
- [5] Martin PJ Lavery, Fiona C Speirits, Stephen M Barnett, and Miles J Padgett, “Detection of a spinning object using light’s orbital angular momentum,” *Science* **341**, 537–540 (2013).
- [6] Severin Fürhapter, Alexander Jesacher, Stefan Bernet, and Monika Ritsch-Marte, “Spiral phase contrast imaging in microscopy,” *Optics Express* **13**, 689–694 (2005).
- [7] Jian Wang, Jeng-Yuan Yang, Irfan M Fazal, Nisar Ahmed, Yan Yan, Hao Huang, Yongxiong Ren, Yang Yue, Samuel Dolinar, Moshe Tur, *et al.*, “Terabit free-space data transmission employing orbital angular momentum multiplexing,” *Nature photonics* **6**, 488 (2012).
- [8] Alois Mair, Alipasha Vaziri, Gregor Weihs, and Anton Zeilinger, “Entanglement of the orbital angular momentum states of photons,” *Nature* **412**, 313 (2001).
- [9] Adetunmise C Dada, Jonathan Leach, Gerald S Buller, Miles J Padgett, and Erika Andersson, “Experimental high-dimensional two-photon entanglement and violations of generalized bell inequalities,” *Nature Physics* **7**, 677 (2011).
- [10] Robert Fickler, Radek Lapkiewicz, William N Plick, Mario Krenn, Christoph Schaeff, Sven Ramelow, and Anton Zeilinger, “Quantum entanglement of high angular momenta,” *Science* **338**, 640–643 (2012).
- [11] Mario Krenn, Marcus Huber, Robert Fickler, Radek Lapkiewicz, Sven Ramelow, and Anton Zeilinger, “Generation and confirmation of a  $(100 \times 100)$ -dimensional entangled quantum system,” *Proceedings of the National Academy of Sciences*, 201402365 (2014).
- [12] R Inoue, T Yonehara, Y Miyamoto, M Koashi, and M Kozuma, “Measuring qutrit-qutrit entanglement of orbital angular momentum states of an atomic ensemble and a photon,” *Physical review letters* **103**, 110503 (2009).
- [13] Dong-Sheng Ding, Zhi-Yuan Zhou, Bao-Sen Shi, and Guang-Can Guo, “Single-photon-level quantum image memory based on cold atomic ensembles,” *Nature communications* **4**, 2527 (2013).
- [14] A Nicolas, L Veissier, L Giner, E Giacobino, D Maxein, and J Laurat, “A quantum memory for orbital angular momentum photonic qubits,” *Nature Photonics* **8**, 234 (2014).
- [15] Zong-Quan Zhou, Yi-Lin Hua, Xiao Liu, Geng Chen, Jin-Shi Xu, Yong-Jian Han, Chuan-Feng Li, and Guang-Can Guo, “Quantum storage of three-dimensional orbital-angular-momentum entanglement in a crystal,” *Physical review letters* **115**, 070502 (2015).
- [16] Dong-Sheng Ding, Wei Zhang, Zhi-Yuan Zhou, Shuai Shi, Guo-Yong Xiang, Xi-Shi Wang, Yun-Kun Jiang, Bao-Sen Shi, and Guang-Can Guo, “Quantum storage of orbital angular momentum entanglement in an atomic ensemble,” *Physical review letters* **114**, 050502 (2015).
- [17] Dong-Sheng Ding, Wei Zhang, Shuai Shi, Zhi-Yuan Zhou, Yan Li, Bao-Sen Shi, and Guang-Can Guo, “High-dimensional entanglement between distant atomic-ensemble memories,” *Light: Science & Applications* **5**, e16157 (2016).
- [18] Wei Zhang, Dong-Sheng Ding, Ming-Xin Dong, Shuai Shi, Kai Wang, Shi-Long Liu, Yan Li, Zhi-Yuan Zhou, Bao-Sen Shi, and Guang-Can Guo, “Experimental realization of entanglement in multiple degrees of freedom between two quantum memories,” *Nature communications* **7**, 13514 (2016).
- [19] Xi-Lin Wang, Xin-Dong Cai, Zu-En Su, Ming-Cheng Chen, Dian Wu, Li Li, Nai-Le Liu, Chao-Yang Lu, and Jian-Wei Pan, “Quantum teleportation of multiple degrees of freedom of a single photon,” *Nature* **518**, 516 (2015).
- [20] Mario Krenn, Mehul Malik, Manuel Erhard, and Anton Zeilinger, “Orbital angular momentum of photons and the entanglement of laguerre-gaussian modes,” *Phil. Trans. R. Soc. A* **375**, 20150442 (2017).
- [21] L-M Duan, MD Lukin, J Ignacio Cirac, and Peter Zoller, “Long-distance quantum communication with atomic ensembles and linear optics,” *Nature* **414**, 413 (2001).
- [22] R Inoue, N Kanai, T Yonehara, Y Miyamoto, M Koashi, and M Kozuma, “Entanglement of orbital angular momentum states between an ensemble of cold atoms and a photon,” *Physical Review A* **74**, 053809 (2006).
- [23] Félix Bussi eres, Nicolas Sangouard, Mikael Afzelius, Hugues de Riedmatten, Christoph Simon, and Wolfgang Tittel, “Prospective applications of optical quantum memories,” *Journal of Modern Optics* **60**, 1519–1537 (2013).
- [24] Khabat Heshami, Duncan G England, Peter C Humphreys, Philip J Bustard, Victor M Acosta, Joshua Nunn, and Benjamin J Sussman, “Quantum memories: emerging applications and recent advances,” *Journal of modern optics* **63**, 2005–2028 (2016).
- [25] Lijun Ma, Oliver Slattery, and Xiao Tang, “Optical quantum memory based on electromagnetically induced transparency,” *Journal of Optics* **19**, 043001 (2017).
- [26] Gavin Brennen, Elisabeth Giacobino, and Christoph Simon, “Focus on quantum memory,” *New Journal of Physics* **17**, 050201 (2015).
- [27] Dong-Sheng Ding, *Broad Bandwidth and High Dimensional Quantum Memory Based on Atomic Ensembles* (Springer, 2017).
- [28] H Jeff Kimble, “The quantum internet,” *Nature* **453**, 1023 (2008).
- [29] Shengwang Du, Jianming Wen, and Morton H Rubin, “Narrowband biphoton generation near atomic resonance,” *JOSA B* **25**, C98–C108 (2008).
- [30] John F Clauser, Michael A Horne, Abner Shimony, and Richard A Holt, “Proposed experiment to test local hidden-variable theories,” *Physical review letters* **23**, 880 (1969).
- [31] Stuart J Freedman and John F Clauser, “Experimental test of local hidden-variable theories,” *Physical Review Letters* **28**, 938 (1972).
- [32] John F Clauser and Michael A Horne, “Experimental consequences of objective local theories,” *Physical review D* **10**, 526 (1974).
- [33] J Leach, B Jack, J Romero, M Ritsch-Marte, RW Boyd, AK Jha, SM Barnett, S Franke-Arnold, and MJ Padgett, “Violation of a bell inequality in two-dimensional orbital angular momentum state-spaces,” *Optics express* **17**, 8287–8293 (2009).
- [34] Jianming Wen and Morton H Rubin, “Transverse effects in paired-photon generation via an electromagnetically induced transparency medium. i. perturbation theory,” *Physical Review A* **74**, 023808 (2006).

- [35] Danielle A Braje, Vlatko Balić, Sunil Goda, GY Yin, and SE Harris, “Frequency mixing using electromagnetically induced transparency in cold atoms,” *Physical review letters* **93**, 183601 (2004).
- [36] M Agnew, J Leach, and RW Boyd, “Observation of entanglement witnesses for orbital angular momentum states,” *The European Physical Journal D* **66**, 156 (2012).